ELSEVIER

Tectonophysics 276 (1997) 19–33

TECTONOPHYSICS

Teleseismic tomography across the middle Urals: lithospheric trace of an ancient continental collision

G. Poupinet [a,*], F. Thouvenot [a], E.E. Zolotov [b], Ph. Matte [c], A.V. Egorkin [b], V.A. Rackitov [b]

[a] *Observatoire de Grenoble et CNRS, B.P. 53X, 38041 Grenoble, France*
[b] *GEON, Chisty 4, Moscow 119034, Russia*
[c] *LGGP, Université Montpellier II et CNRS, Place Eugène-Bataillon, 34095 Montpellier, France*

Received 7 May 1996; accepted 10 December 1996

Abstract

The Urals are a major collision belt between two continental plates separated by island arcs: the East European plate and the Siberian plate. Their linear structure is preserved on a length of about 3000 km. A seismic array of 61 stations has been deployed during more than 3 months on a linear profile across the middle Urals, north of Ekaterinburg. P-wave travel-time residuals are inverted and provide a tomographic cross-section of the lithosphere on a 600-km-long profile across the Urals. An east–west asymmetry is observed both in the crust and in the lithosphere: the western limit between these two different lithospheres corresponds to the western front of the Uralian orogen from the surface to a depth greater than 100 km. Several crustal studies were performed by other teams along the same profile, and we compare our teleseismic cross-section to common-depth-point seismics, to deep seismic soundings and to a wide-angle-reflection fan profile. East of the main Uralian fault, the teleseismic inversion shows high-velocity bodies corresponding to well-known volcanic/mafic and ultramafic rocks in the Tagil syncline. These high-velocity bodies do not appear to be rooted in the lower crust. As a whole, the teleseismic tomogram comforts the Moho imbrication model proposed by Juhlin et al. (1995).

Keywords: body waves; structure of the crust; structure of the lithosphere and mantle; continental tectonics; Europe; tomography

1. Introduction

The Urals are a linear mountain belt extending N–S for 3000 km from Novaya Zemlya to the Aral Sea. They were formed during the Carboniferous–Permian (345–230 Ma) by the collision of the Baltic shield (East European plate) with the Siberian plate and related microblocks and volcanic arcs in between (Hamilton, 1970; Zonenshain et al., 1984; Matte, 1995). The collision between the two plates involved the accretion of several volcanic arcs and the obduction of ophiolites. Some of the largest and most extensive ophiolite belts in the world are exposed there. At variance with several other mountain ranges of comparable age, like the Variscides, the Appalachians and the Caledonides, the Urals were not significantly remobilized after the Jurassic. Therefore they are one of the best preserved Palaeozoic orogens.

From west to east on a transect at the latitude of our profile (58°N), the following geological units are crossed (Figs. 1 and 2): (a) the East European plate,

* Corresponding author. Fax: +33-476-828101.

0040-1951/97/$17.00
PII S0040-1951(97)00045-0

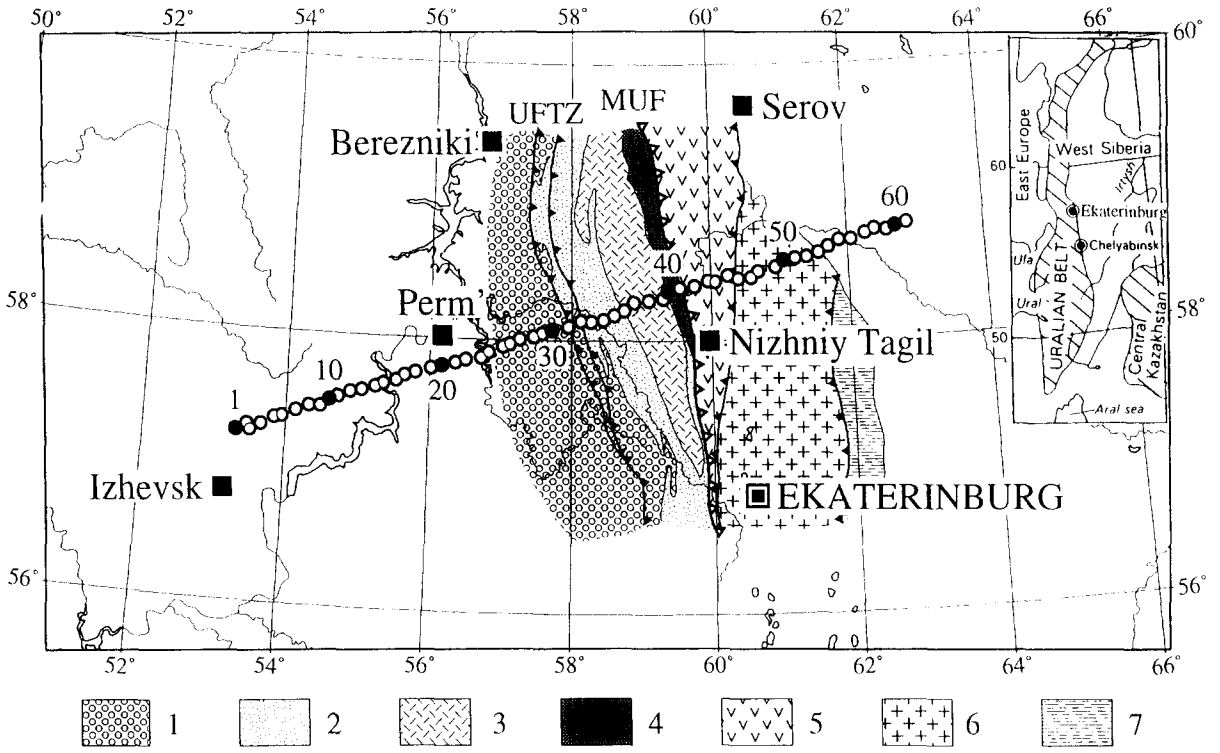

Fig. 1. Profile location in the middle Urals. Besides recording a deep-seismic-sounding experiment, the 61 stations recorded teleseismic events during 3 months. Sketch of geology is drawn on the Uralian part of the profile. *1* = Permian Uralian foredeep; *2* = Palaeozoic and Vendian sediments of the Uralian frontal thrust zone (UFTZ); *3* = Kvarkush Riphean anticlinal stack; *4* = high-pressure zone and Main Uralian fault (MUF); *5* = Tagil synform; *6* = Salda granitic antiform; *7* = eastern Uralian zone.

with the Uralian foredeep along its eastern boundary; (b) the Palaeozoic and Vendian sediments of the Uralian frontal thrust zone (UFTZ); (c) the Kvarkush anticline; (d) the Main Uralian fault (MUF); (e) the Tagil synform; (f) the Salda antiform; and (g) the eastern Uralian zone (Ivanov et al., 1975).

From a geophysical point of view, the Urals have been extensively investigated. The Bouguer gravity map shows a +50-mGal linear high running along the 60°E meridian flanked by two long-wavelength Bouguer lows (−50 mGal). Kruse and McNutt (1988) interpret this anomaly high as resulting from high-density ultramafic rocks and high-pressure mafic-rock units in the upper crust (0.1–0.15 g/cm^3 higher than average crustal density). A similar N–S linear trend is observed in the aeromagnetic map. An extremely low value of heat flow (25 mW/m^2) is measured in the centre of the chain and may result from the same peculiar composition of the upper crust (Hurtig et al., 1992).

More than 20 seismic studies, usually deep-seismic-sounding (DSS) experiments have been performed by Russian teams across the Urals since 1983; several profiles intersect in the region of the Urals superdeep borehole (see Ryzhiy et al., 1992; Kashubin et al., 1995). In DSS experiments, explosions of various sizes were shot along a profile from which the hodochrons of direct, refracted, and reflected P- and S-waves were obtained. The result of a DSS profile is a composite cross-section of the crust giving velocities of P- and S-waves at various depths and the main fracture zones. When available, common-depth-point (CDP) reflection data on intersecting profiles are also used in DSS interpretations. P-waves converted to S-waves from distant earthquakes provide additional constraints on the main crustal interfaces.

Recently several crustal studies have been performed across the middle Urals on or near the profile of our teleseismic study:

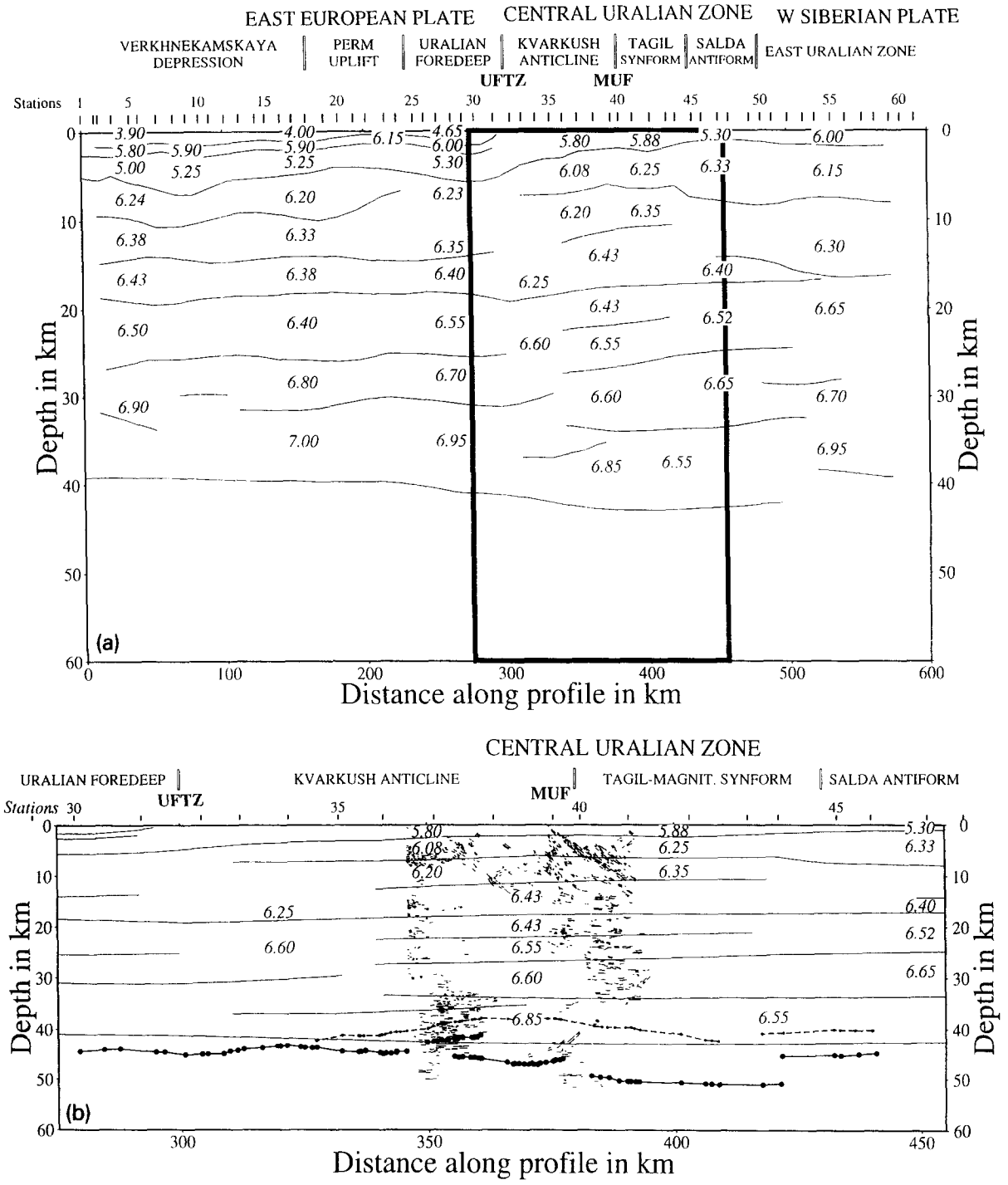

Fig. 2. (a) Crustal cross-section along the profile as obtained by GEON from deep-seismic-sounding results. Interfaces are given as thin lines and P-wave velocities in km/s are indicated in each unit. Schematic description of the main geological units shown on top. (b) Blow-up of the box in (a). GEON DSS results same as (a). Short light lines are the main reflectors obtained by Juhlin et al. (1995) in their migrated CDP time-section. (Time-to-depth conversion was computed using a normal-move-out velocity increasing from 6 km/s in surface to 6.5 km/s at the base of the crust.) Dots show the wide-angle reflections obtained by Thouvenot et al. (1995) from a fan profile fired to detect the crustal root of the Urals (large dots = Moho; small dots = intracrustal reflection). CDP and wide-angle data were projected onto the profile along the strike of the geological units (here oriented N–S), since they were obtained 60 km to the south.

(1) A 600-km-long refraction/reflection profile by GEON (Egorkin, 1995) was carried out exactly on the site of the teleseismic profile.

(2) A 120-km-long CDP line (Juhlin et al., 1995) intersects the DSS profile at the Urals superdeep borehole in the Tagil synform, where a maximum drilling depth of 4.3 km was reached.

(3) A wide-angle-reflection fan profile mapped the crustal root of the Urals (Thouvenot et al., 1995), with reflection points on the Moho positioned 60 km south of the teleseismic profile.

These crustal profiles use different techniques and complement each other in the description of the deep crust (Fig. 2). The crustal thickness (at least 40 km) is similar beneath the East European platform and beneath the Siberian platform. It increases by up to 3–5 km beneath the central part of the orogen (Egorkin, 1995), thus delineating a crustal root similar to that found by Thouvenot et al. (1995) further south. The actual presence or absence of a root beneath the Urals has long been the object of a debate because it has implications on the mechanism of isostatic compensation (Kruse and McNutt, 1988). The average surface-to-Moho P-wave velocity increases from 6.15 km/s beneath the East European platform to 6.45 km/s beneath the Urals, with also a slight increase in the mean crustal velocity from the west (6.3 km/s) to the east (6.55 km/s) of the central Uralian zone. Similar results were found for the Moho geometry and average velocities on the regional profile RUBIN-2 performed by GEON in 1988.

The cross-section of the crust derived by GEON (Egorkin, 1995) is presented in Fig. 2a. In Fig. 2b, a close-up of the central part of Fig. 2a, we added the main reflectors found by Juhlin et al. (1995) and by Thouvenot et al. (1995). Station locations are indicated by their index, from 1 to the west to 61 to the east. Tectonic units are identified on top of the figure, from the East European platform to the west to the West Siberian basin to the east. In this interpretation, the crust appears as the juxtaposition of blocks with slightly different properties.

The East European platform is characterized by an Archaean crystalline basement covered by thick sediments (up to 15 km) from Riphean to Permian in age. The basement is built from granulitic gneisses and pierced by granitoids and other Proterozoic intrusives. It outcrops in the Central Urals where U/Pb ages from metamorphic zircons suggest a granulite-facies metamorphism ca. 2600 Ma (Lennykh, 1980). The thickness of the sedimentary layer varies laterally and thins when approaching the Urals from the west (station 32). The Uralian foredeep is built of Permian molasse overlapping Palaeozoic deposits.

Within the Palaeozoic complex of the Urals, several anticlinal and synclinal zones are identified: the Kvarkush anticline on the western side (stations 32–40) is characterized by extensive development of Devonian and Carboniferous carbonate cover and a core of Vendian to Riphean sediments (Ministry of Geology SSSR, 1966). The whole zone is thrusted to the west onto the Uralian foredeep. Rocks of Archaean age may correspond to the layer which reflects energy from a depth of 7–8 km. On the profile of Juhlin et al. (1995), the lower crust of the central part of the Kvarkush anticline is reflective but the eastern part of the same unit appears transparent. On the fan profile of Thouvenot et al. (1995), reflections from the Moho are shifted upwards and downwards in the same zone of the profile (between km 350 and 360 of Fig. 2b): both PmP and SmS reflections show the same complexity. This feature seems to correspond to a lower crustal flake, in which the P-wave velocity reported by GEON is low, only 6.55 km/s at a depth of 35 km.

The MUF is located near station 40. In Juhlin et al. (1995), the MUF is the most striking feature: it can be traced down as a reflection horizon to a depth of the order of 15 km. Moreover, energy is reflected from the Moho (at about 50 km) vertically beneath the surface trace of the MUF, where the lower crust is also reflective. On GEON's DSS profile, different crustal blocks are observed on both sides of stations 32–34. However, the MUF, which is so predominant in the CDP reflection profile, is not clearly observed by DSS.

The Tagil synform (stations 40–45) is characterized by volcanic formations, sub-continental basaltoids and Upper-Silurian and Early-Devonian terrigenous sediments. The first refractive boundary at a depth of 3 km in Fig. 2b coincides with the surface of a high-velocity sub-complex also identified by the Urals superdeep borehole (located between station 41 and station 42) (Juhlin et al., 1995). A change in average crustal velocity and in V_P/V_S (which gives the maficity index) is observed beneath the Tagil synform where mafic rocks are exposed. To the east,

the Salda antiform is dated from the Palaeoproterozoic and forms the eastern slope of the Urals. Under the Salda antiform (stations 45–49) at a depth of 1 km, a tentatively Archaean basement surface is identified. The eastern Uralian zone (stations 50–60) corresponds to the West Siberian plate. The Moho is seen at a depth of 40 km beneath the Siberian platform.

2. Teleseismic data across the middle Urals

A linear array of 61 seismic stations with a 10-km spacing was set up for a three-month period along a line across the middle Urals north of Ekaterinburg (Table 1 and Fig. 1). Each station consisted of a 3-component 1.5-s seismometer and a recorder. The seismic signal was continuously recorded on an analog magnetic tape with slow-speed recording — the Cherepakha seismic recorder. The main advantage of this equipment is that it is recording continuously. The equipment belongs to GEON and has been used for most of the very-long-range seismic profiles in the former Soviet Union. The Cherapakha recorder is equipped with a quartz clock and time comparisons with a radio-driven master clock were performed every week when the tapes were retrieved. After correction for drifts, a timing precision of the order of 0.01–0.02 s is maintained. Usually GEON deploys the Cherepakha equipment during one or two weeks to study converted phases in the teleseismic P-coda. For this teleseismic tomographic experiment, Cherepaka stations were maintained in the same location for a longer time period; this experiment was performed in the frame of the Europrobe project and of the French CNRS Lithoscope programme.

70 teleseismic events were recorded; they were

Table 1
Coordinates of the seismological stations deployed by GEON across the middle Urals for this teleseismic study

Station	Latitude	Longitude	Altitude (m)
01	57°15.03′N	53°18.30′E	180
02	57°17.93′N	53°27.18′E	140
03	57°15.50′N	53°30.00′E	150
04	57°18.33′N	53°39.00′E	160
05	57°21.63′N	53°50.20′E	190
06	57°22.45′N	53°56.35′E	175
07	57°25.40′N	54°08.02′E	257
08	57°27.68′N	54°18.88′E	140

Table 1 (continued)

Station	Latitude	Longitude	Altitude (m)
09	57°27.87′N	54°28.37′E	120
10	57°30.95′N	54°35.82′E	170
11	57°32.58′N	54°42.85′E	127
12	57°34.98′N	54°53.17′E	180
13	57°36.02′N	55°03.18′E	250
14	57°37.78′N	55°14.55′E	200
15	57°39.37′N	55°21.00′E	100
16	57°40.78′N	55°31.85′E	120
17	57°43.18′N	55°38.83′E	120
18	57°44.68′N	55°47.88′E	242
19	57°46.73′N	56°01.08′E	300
20	57°48.18′N	56°10.15′E	170
21	57°49.58′N	56°21.42′E	130
22	57°51.08′N	56°30.17′E	210
23	57°52.03′N	56°43.15′E	170
24	57°54.47′N	56°49.67′E	180
25	57°57.08′N	57°01.70′E	200
26	57°58.33′N	57°07.67′E	160
27	58°00.28′N	57°16.03′E	167
28	58°01.37′N	57°28.00′E	242
29	58°02.97′N	57°35.30′E	180
30	58°04.50′N	57°43.57′E	225
31	58°06.02′N	57°57.15′E	380
32	58°08.45′N	58°07.67′E	260
33	58°08.12′N	58°16.67′E	260
34	58°08.95′N	58°27.00′E	240
35	58°10.92′N	58°36.47′E	290
36	58°12.95′N	58°45.18′E	325
37	58°16.40′N	58°53.37′E	455
38	58°17.23′N	59°06.25′E	420
39	58°18.05′N	59°18.37′E	380
40	58°21.30′N	59°22.67′E	350
41	58°22.55′N	59°32.65′E	280
42	58°23.48′N	59°45.65′E	220
43	58°25.68′N	59°57.40′E	220
44	58°25.30′N	60°03.50′E	198
45	58°27.92′N	60°14.50′E	180
46	58°26.60′N	60°23.47′E	150
47	58°26.98′N	60°34.82′E	140
48	58°29.73′N	60°41.23′E	140
49	58°31.52′N	60°56.30′E	140
50	58°34.42′N	61°03.43′E	110
51	58°35.20′N	61°13.67′E	142
52	58°35.82′N	61°23.83′E	120
53	58°37.40′N	61°34.53′E	135
54	58°39.87′N	61°43.20′E	118
55	58°42.83′N	61°52.83′E	125
56	58°42.98′N	62°03.17′E	85
57	58°45.30′N	62°15.87′E	90
58	58°46.97′N	62°24.08′E	80
59	58°46.30′N	62°34.68′E	105
60	58°47.93′N	62°42.33′E	110
61	58°49.05′N	62°52.50′E	90

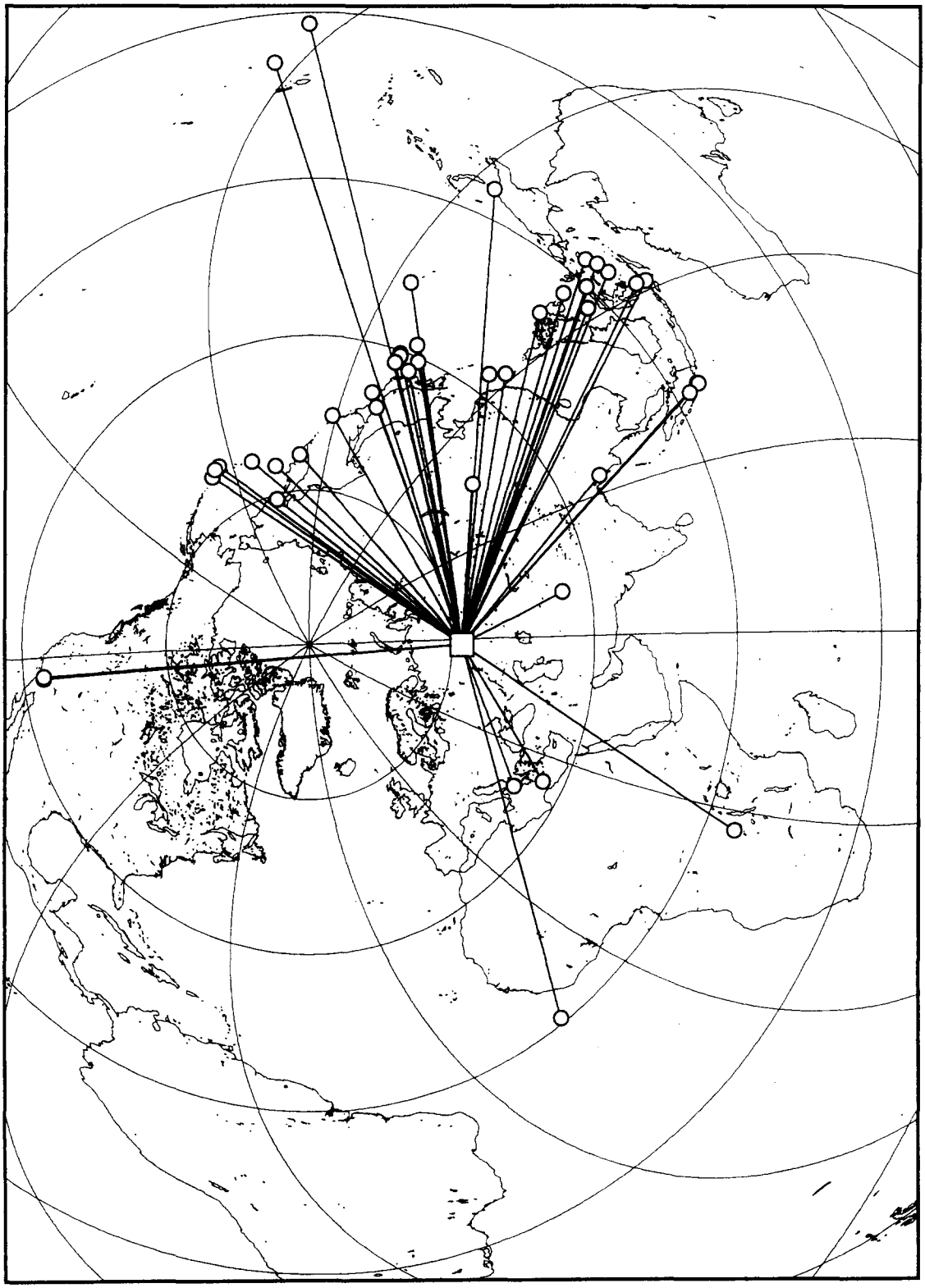

Fig. 3. Distribution of events used for the computation of the P-wave residuals and for the inversions. Notice that most events arrive in the NE and SE quadrants.

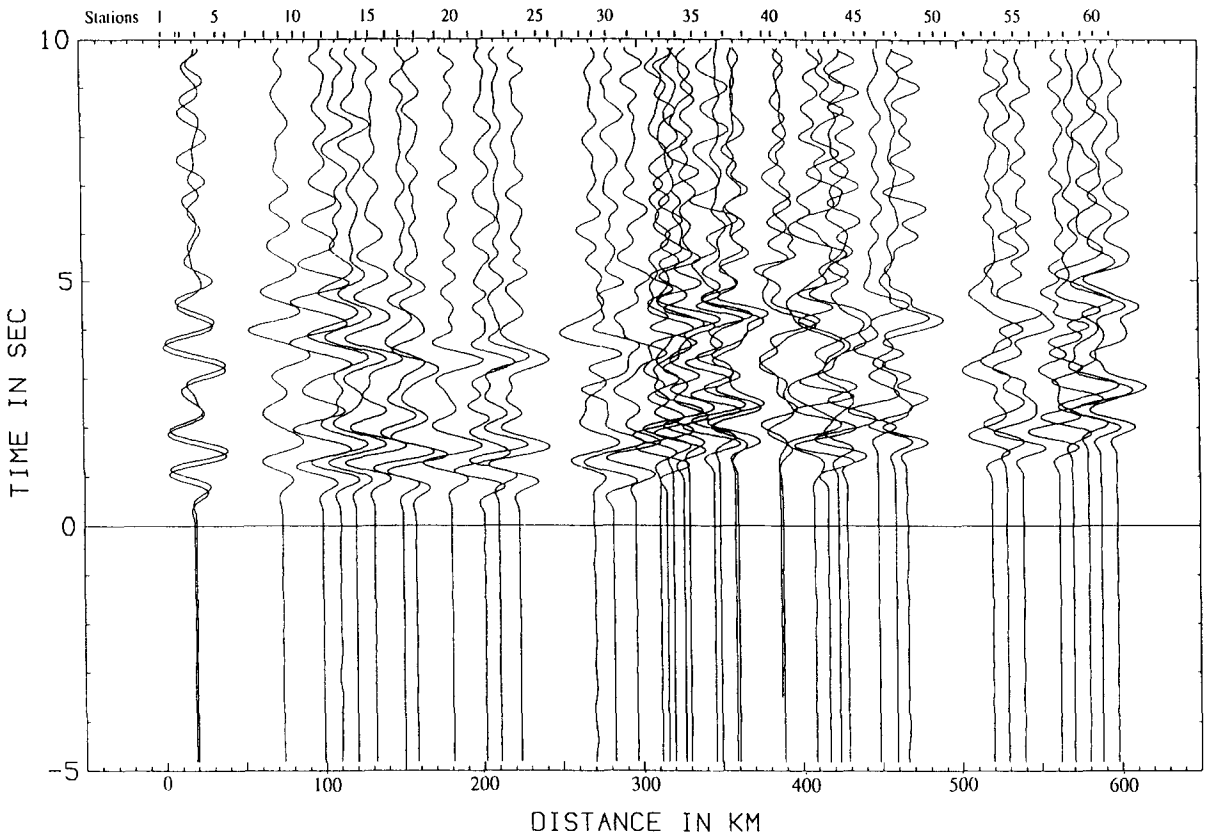

Fig. 4. Example of records of the vertical component for an earthquake that occurred on September 19th 1992 at 19:19:07.5, south of Honshu. On the distance axis, 0 marks the centre of the recording array (58°N, 58°E).

digitized and most had clear first arrivals. The geographical distribution of events is shown in Fig. 3. Most events originate in the NE and SE quadrants. P-wave arrival times were determined by visual waveform correlation: a precision of about 0.05–0.08 s in picking P-waves is obtained (see Fig. 4, for example). P-wave travel-time residuals were computed with respect to the Herrin tables (Herrin, 1968) using NEIC Preliminary Determinations of Epicentres. In order to reduce bias due to source mislocations, origin-time errors, and lower-mantle heterogeneities, relative residuals were computed with respect to the average residual for each earthquake. Henceforth, when we refer to 'P-wave residuals' in the following text, this term should be understood as 'P-wave travel-time relative residuals'.

P-wave residuals for individual earthquakes from different source regions are in the general range ±0.5 s. In Fig. 5, the average P-wave residual is computed for each station. In the crust, seismic rays for a given station remain in a narrow cone whose properties are nearly constant (see Fig. 6). The stations fall into three groups: stations 1–32 (East European plate), stations 33–50 (central Uralian zone), and stations 51–61 (West Siberian plate). The average P-wave residuals are, respectively, −0.1 s, +0.3 s and 0 s in each unit. We notice some correlation between the P-wave residuals pattern and geological units (see for instance in Fig. 5 the short-wavelength anomaly near stations 40–45 located in the Tagil synform). These units have slightly different average properties and/or different mineralogical compositions. When we compute crustal vertical travel-times for each station from GEON refraction results, we obtain a maximum vertical travel-time difference of 0.15 s. This value is smaller than what we observe in Fig. 5, so that a part of the observed station residuals is caused by subcrustal structure variations.

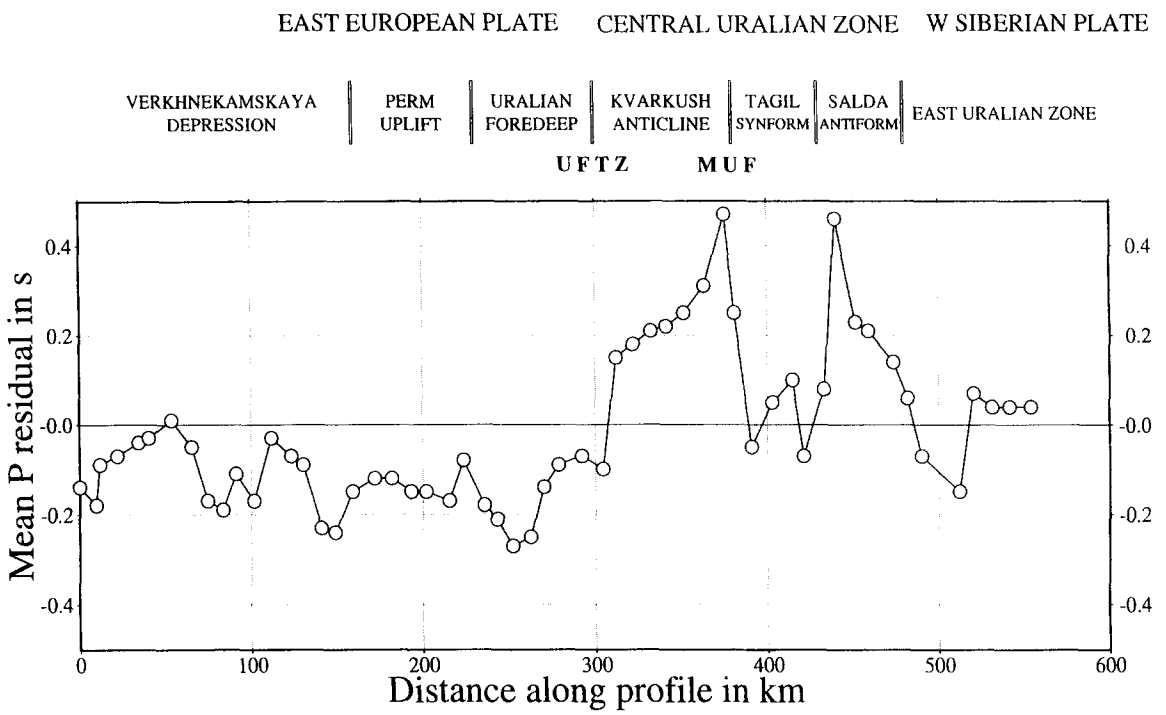

Fig. 5. Average P-wave residuals for each station. Error on each residual around 0.1 s.

The distribution of P-wave residuals as a function of azimuth for the central part of the profile is presented in Fig. 6, which shows the clear contrast to the west and to the east of station 32.

3. Tomographic inversion of the data

P-wave residuals are integrals of time anomalies generated by heterogeneities along the entire ray-path. Rays originating from the same source become separated only in the crust and in the uppermost mantle beneath the stations. Hence, P-wave residuals yield information on crustal and lithospheric velocities beneath the array. The narrow longitudinal aspect of the Urals and the fact that most geophysical fields (e.g., gravity or aeromag) exhibit the same longitudinal shape seem to imply that a cross-section may be a reasonable first-order image of the Uralian deep structure. We inverted our P-wave-residuals data set with the ACH technique (Aki et al., 1977; Ellsworth, 1977). Evans and Achauer (1992) introduced modifications to the original algorithm and their program AVTHRD was used. Two sets of data have been considered in the inversion: (1) the complete set of P-wave arrivals, and (2) a selection of events whose azimuth is close to that of the profile. Both sets were inverted in order to test the quality and stability of the tomographic image. Most inversions give very similar results: the complete data set contains more short-wavelength features that may not be relevant in such a first-order study. Following Evans and Achauer (1992), inversions were performed using individual cones beneath each station. Thus the delay due to the sub-surface is introduced as a variable in the inversion. Our starting model is given in Table 2. As usual, the inversion does not vary significantly with differ-

Table 2
Starting model for inversion of Table 3 and Fig. 6

Starting model for inversion		
N	V_P (km/s)	H (km)
1	6.20	20.0
2	6.60	25.0
3	8.20	50.0
4	8.30	50.0
5	8.40	50.0
6	8.50	50.0

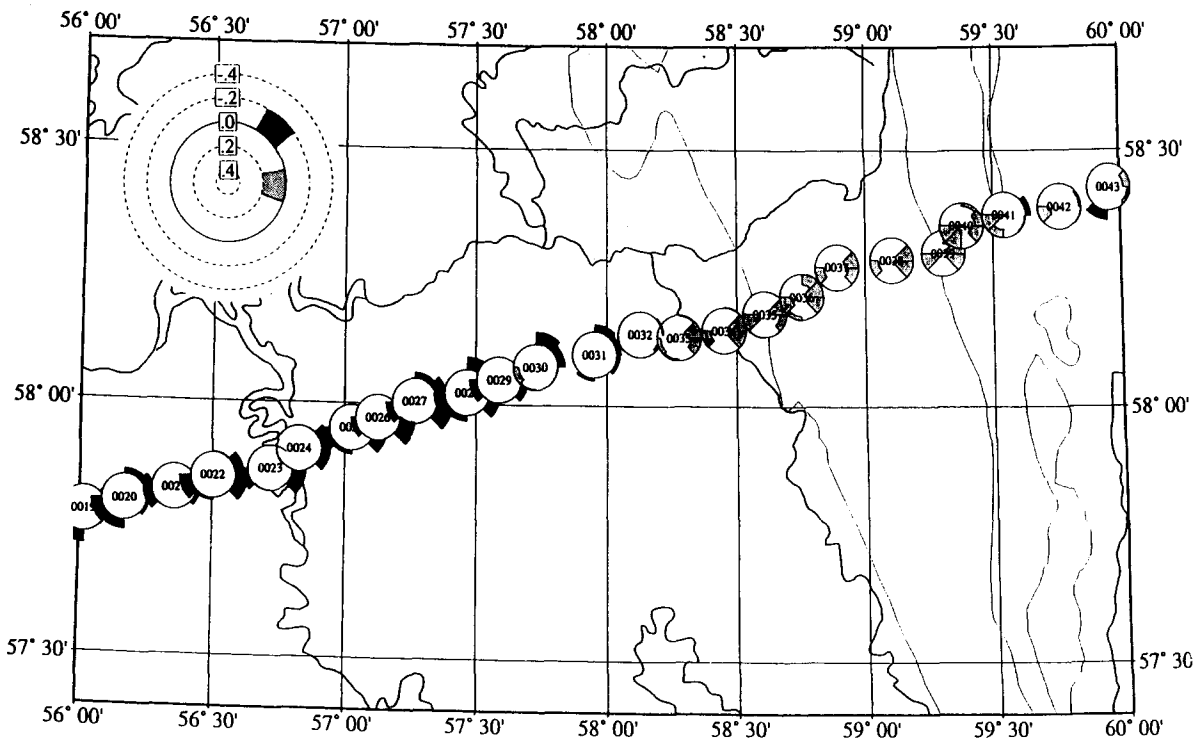

Fig. 6. P-wave residuals as a function of the earthquake back-azimuth for stations situated on both sides of the Uralian frontal thrust zone. Circle corresponds to a zero P-wave residual. The numbers inside the circles correspond to station numbers. Positive P-wave residuals are indicated as values inside the circle (light shade) and negative P-wave residuals as values outside the circle (black).

ent initial models. Twenty-km-wide and 300-km-long blocks were taken perpendicular to the profile. The perturbations in velocity derived from the various inversion schemes are rather small (<2%), as expected because the P-wave residuals were small. The improvement in variance is of the order of 70%. The 2-D model can be viewed as an integrated picture of the structures perpendicular to the profile.

A typical tomographic image is presented in Table 3 and in Fig. 7. In Table 3, we list the index of each block, the P-wave velocity perturbation in per cent, the number of rays in each block, the diagonal element of the resolution matrix, and a standard error on the velocity perturbation. A negative value of the velocity perturbation corresponds to a velocity smaller than the starting model. For instance, a thinner crust appears as a faster block in this presentation (i.e., a positive number or green–blue colour). For this inversion, the improvement in variance is 71%, leaving a residual variance of about 0.02 s^2 or about 0.14 s of signal unexplained. Despite serious limitations related to the fact that no exact ray tracing was performed, the resolution matrix is the usual measurement to quantify how the velocity perturbation is resolved in a block; according to Kissling (1988), it is however essentially related to the number of hits per cell. In Table 3, the diagonal terms of the resolution matrix are close to 0.5–0.6; this is not exceptional and may be due to the limited azimuthal coverage. Most blocks in the centre of the profile are properly resolved because the central blocks are criss-crossed by rays. The standard errors are in the 0.40–0.45% range, i.e., less than most observed anomalies (1–1.5%). The various inversions give consistent velocity cross-sections, all very similar to the results of Fig. 7 which were obtained by selecting events with azimuths close to that of the profile.

4. Discussion and conclusion

The joint consideration of several crustal profiles using different techniques and of a teleseismic inver-

Table 3
Results of the inversion for the P-wave residuals collected along the profile

1	2	3	4	5	6	7	8	9	10	11	12	13	14	15	16	17	18
			0.12	0.88	−1.41	−0.19	2.06	0.67	0.95	1.37	1.05	0.87	0.44	0.92	1.54	0.41	1.09
			46	54	43	53	51	27	32	31	21	23	41	52	43	34	36
			0.343	0.359	0.344	0.401	0.438	0.351	0.405	0.427	0.393	0.358	0.389	0.409	0.399	0.400	0.413
			0.42	0.45	0.41	0.43	0.45	0.46	0.45	0.46	0.47	0.46	0.45	0.45	0.46	0.44	0.45
36	37	38	39	40	41	42	43	44	45	46	47	48	49	50	51	52	53
			1.55	1.25	0.40	−0.09	0.53	0.76	1.09	0.81	1.55	0.48	1.02	1.17	0.96	1.05	0.32
			17	52	41	48	54	38	31	48	34	26	28	35	45	36	44
			0.302	0.382	0.423	0.482	0.459	0.433	0.409	0.388	0.385	0.406	0.457	0.497	0.467	0.425	0.415
			0.44	0.41	0.42	0.44	0.42	0.45	0.44	0.44	0.46	0.43	0.43	0.44	0.44	0.46	0.45
71	72	73	74	75	76	77	78	79	80	81	82	83	84	85	86	87	88
				0.96	2.30	0.46	0.27	1.93	0.79	0.61	2.24	0.95	0.71	0.48	0.77	0.83	0.36
				41	69	76	74	74	62	50	59	51	44	53	68	62	58
				0.475	0.547	0.0546	0.563	0.519	0.535	0.534	0.481	0.495	0.472	0.537	0.550	0.561	0.558
				0.46	0.42	0.40	0.40	0.42	0.42	0.42	0.40	0.40	0.42	0.41	0.42	0.42	0.42
106	107	108	109	110	111	112	113	114	115	116	117	118	119	120	121	122	123
				−0.52	1.07	0.25	0.83	0.37	0.68	−0.22	0.58	0.62	0.46	−0.41	−0.19	−0.83	−0.23
				11	29	60	78	72	76	72	61	57	52	46	52	54	65
				0.422	0.465	0.545	0.548	0.559	0.533	0.585	0.499	0.451	0.473	0.486	0.561	0.557	0.537
				0.49	0.45	0.41	0.43	0.43	0.42	0.41	0.41	0.40	0.40	0.42	0.43	0.43	0.43
141	142	143	144	145	146	147	148	149	150	151	152	153	154	155	156	157	158
				−0.06	0.40	−0.74	−0.43	0.07	0.48	−0.87	−0.49	−0.27	−0.62	−0.60	−0.69	0.93	−0.13
				11	12	22	53	74	78	72	71	56	48	56	53	52	59
				0.368	0.306	0.465	0.545	0.576	0.569	0.584	0.543	0.474	0.469	0.509	0.523	0.551	0.577
				0.45	0.42	0.46	0.44	0.42	0.41	0.42	0.43	0.43	0.42	0.42	0.44	0.43	0.44
176	177	178	179	180	181	182	183	184	185	186	187	188	189	190	191	192	193
			2.36	0.87	−0.96	−0.95	−0.90	−2.20	−1.01	−2.08	−0.93	−0.58	−0.56	−0.48	−0.04	0.39	0.08
			11	10	14	17	23	38	63	73	76	70	66	53	58	62	52
			0.248	0.334	0.401	0.428	0.546	0.621	0.596	0.614	0.625	0.603	0.555	0.529	0.564	0.647	0.550
			0.40	0.47	0.48	0.48	0.48	0.45	0.46	0.45	0.45	0.45	0.47	0.47	0.47	0.44	0.48

Table 3 (continued)

19	20	21	22	23	24	25	26	27	28	29	30	31	32	33	34	35
−1.59	−1.41	−0.13	−3.20	1.57	0.88	−0.250	−0.75	0.24	1.20	−0.23	−0.88	−0.209	−0.155			
36	50	38	36	23	38	28	43	56	32	48	43	49	47			
0.375	0.418	0.334	0.405	0.376	0.433	0.406	0.419	0.413	0.287	0.377	0.333	0.367	0.336			
0.45	0.45	0.46	0.44	0.46	0.45	0.45	0.45	0.43	0.44	0.43	0.44	0.43	0.38			
54	55	56	57	58	59	60	61	62	63	64	65	66	67	68	69	70
−0.09	−1.49	−1.89	−2.46	1.63	−1.22	0.17	−2.19	−0.05	1.35	−0.98	−0.40	−0.39	−1.80	−1.66		
36	43	41	44	37	38	46	45	53	40	37	44	43	49	23		
0.411	0.476	0.466	0.381	0.438	0.393	0.415	0.435	0.402	0.446	0.434	0.453	0.445	0.446	3.11		
0.45	0.44	0.44	0.45	0.45	0.44	0.41	0.41	0.42	0.43	0.43	0.43	0.43	0.41	0.39		
89	90	91	92	93	94	95	96	97	98	99	100	101	102	103	104	105
−0.43	−1.33	−1.88	−1.37	−0.79	−1.27	−0.02	−0.61	−1.99	−0.78	0.00	−1.30	−0.91	−0.15	−1.96	−1.90	
57	59	67	65	65	51	51	58	57	80	63	67	69	69	65	33	
0.567	0.546	0.568	0.479	0.555	0.512	0.536	0.552	0.507	0.550	0.519	0.526	0.546	0.469	0.362	0.272	
0.42	0.42	0.41	0.43	0.42	0.44	0.43	0.40	0.41	0.39	0.40	0.39	0.41	0.39	0.33	0.28	
124	125	126	127	128	129	130	131	132	133	134	135	136	137	138	139	140
0.76	0.17	0.97	−0.66	−2.04	−1.17	−0.72	−0.43	−1.27	−1.47	−1.33	−0.97	0.99	0.28	−0.32	−1.19	−2.05
64	55	58	64	62	60	43	58	58	67	75	68	62	60	64	56	40
0.553	0.521	0.557	0.509	0.536	0.495	0.526	0.453	0.518	0.542	0.514	0.498	0.444	0.462	0.427	0.389	0.394
0.44	0.43	0.43	0.42	0.42	0.43	0.42	0.42	0.41	0.42	0.41	0.40	0.42	0.41	0.40	0.34	0.39
159	160	161	162	163	164	165	166	167	168	169	170	171	172	173	174	175
0.11	−0.24	0.58	0.72	0.00	−0.71	−1.24	−2.01	−0.46	−1.22	−0.33	−0.03	0.04	−0.54	0.53	−0.23	0.15
64	61	55	51	55	66	59	56	54	59	59	60	71	62	67	61	62
0.538	0.542	0.521	0.500	0.462	0.516	0.492	0.452	0.507	0.518	0512	0.505	0.439	0.456	0.463	0.392	0.448
0.44	0.44	0.44	0.42	0.43	0.42	0.44	0.42	0.40	0.41	0.41	0.42	0.40	0.41	0.39	0.36	0.42
194	195	196	197	198	199	200	201	202	203	204	205	206	207	208	209	210
−0.03	1.06	0.11	0.14	−0.21	0.15	−0.17	−0.68	−0.42	−0.82	0.41	0.22	−0.43	−0.78	−0.01	−0.81	−1.00
50	52	57	60	50	55	57	66	59	53	58	51	56	64	66	66	60
0.622	0.591	0.595	0.590	0.549	0.565	0.576	0.572	597	0.581	0.609	0.555	0.515	0.546	0.558	0.527	0.500
0.47	0.47	0.46	0.47	0.46	0.47	0.46	0.46	45	0.46	45	46	49	46	43	46	45

The centre of the array of blocks is located at 58°N and 58°E, near station 31. For each block, we print: (1) the index of the block in the inversion; (2) the P-wave velocity perturbation in per cent; (3) the number of rays crossing the block; (4) the diagonal element of the resolution matrix; (5) the standard error on the P-wave velocity perturbation.

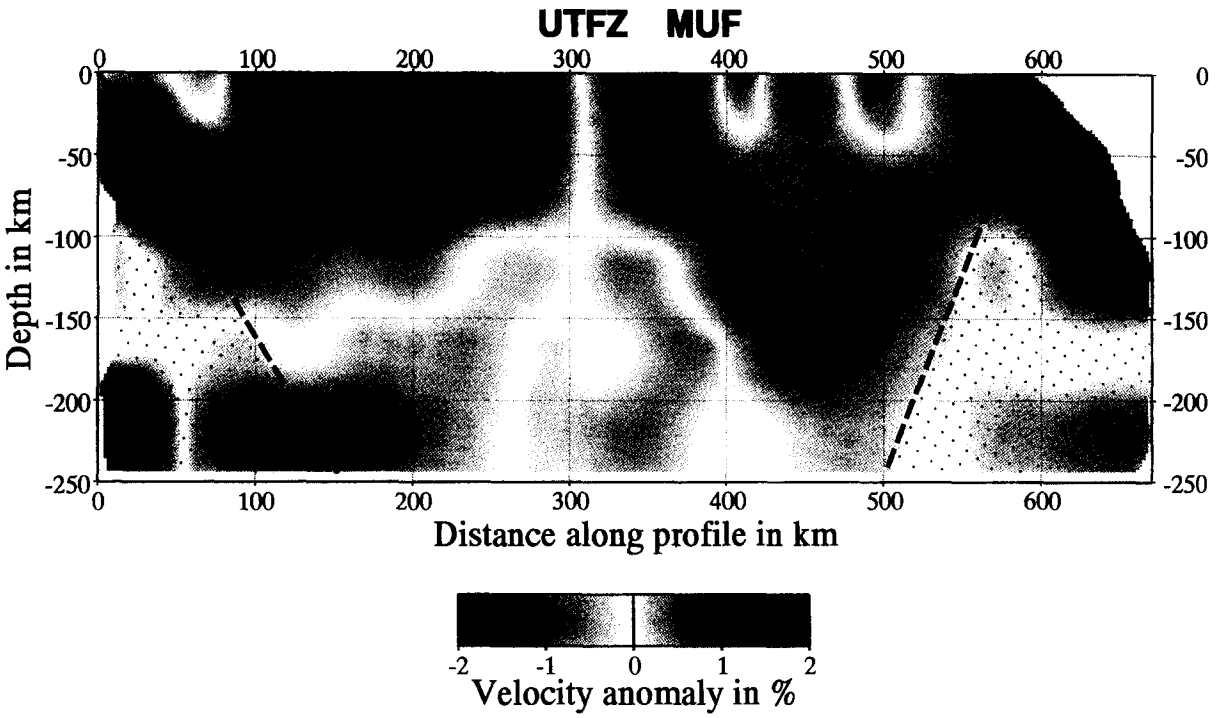

Fig. 7. Vertical cross-section of the lithosphere along the middle-Urals profile resulting from the inversion of P-wave residuals. The colour scale shows velocity perturbations relatively to the average model given in Table 3. A positive (green–blue colour) perturbation means that the velocity is higher than the starting model in this place. The western and eastern ends of the figure marked by black dots correspond to the part of the model which is less resolved because rays do not criss-cross the blocks as they do in the central part.

sion shows that these imaging techniques supplement each other to better constrain tectonic models of the formation of a mountain range. While reflection and wide-angle seismics map the main interfaces in the crust, DSS characterizes velocities inside the crustal units defined by reflections. The teleseismic inversion constrains the average velocity of lithospheric blocks and marks boundaries between the plates that participated in the collision.

Three main points can be considered here for discussion.

(1) The lithosphere down to a depth of 100 km across the middle Urals can be divided into two main segments: a high-velocity segment (green–blue) to the west (East European plate) and a low-velocity segment (orange–red) to the east. An average velocity contrast of 2–3% distinguishes these two main units. Their limit is near station 32, close to the UFTZ which corresponds to the western front of the Urals. This limit is clearly shifted to the west of the MUF (station 39).

(2) In the eastern part of the profile, two 30–40-km-wide high-velocity (+3%) bodies are detected in the crust. The western one correlates with the Tagil synform composed of mafic material. These high-velocity bodies do not seem to extend to the Moho. The lower-velocity zone between these two high-velocity bodies seems to correspond to the Salda granito-gneissic antiform made of continental crust.

(3) If we consider that the lithosphere beneath the East European platform has a thickness of the order of 130–150 km, the subcrustal lithosphere beneath the Urals is characterized by lower velocities than in the shield area or is thinner.

If the vergence of a palaeo-subduction was inferred from the tomographic image, the east-dipping border of the Uralian plate would favour a corresponding east-dipping subduction. However, with the limited resolution of this teleseismic experiment, it is sounder to state that the contact between the East European and the Uralian plates deeps eastwards very steeply to a depth of more than 100 km.

From their CDP seismic reflection study, Juhlin et al. (1995) find that the MUF is dipping eastward

(see Fig. 2b). Strong reflections are observed in the hanging wall. They also find east-dipping reflectors in the Precambrian phyllites of the Kvarkush unit which appears thus as an anticlinal stack. The middle crust beneath the MUF is reflective. This reflectivity shallows west of the MUF. Deep reflections from around 50 km just below the surface trace of the MUF probably correspond to the Uralian crustal root. The main question is to know which Moho (East European platform Moho or Uralian Moho) lies there. Using various hypotheses on the nature of the reflecting Moho, Juhlin et al. (1995) propose three possible tectonic interpretations: (1) a no-crustal-root model, in which an island-arc limited to the west by the MUF overrides the European lower crust; (2) a Moho-imbrication model, a piece of reflective lower crust from the East European platform is imbricated in the Uralian plate and the root of the Urals would be a modified upper-mantle body coming from the east; and (3) a crustal-intercalation model, the suture zone has a zigzag shape separating the East European and the Uralian crust. The East European plate would be in contact with the island-arc crust at the vertical of the MUF.

How does the teleseismic tomogram relate to these proposed tectonic interpretations of the CDP data by Juhlin et al. (1995)? At subcrustal depth, the contact between the East European plate and the plate that supports the Urals is in a position which is clearly to the west of the surface trace of the MUF. The average velocity in the plate beneath the Urals is lower than the velocity in the plate beneath the East European platform. The lithospheric block beneath the Urals sensu stricto does not appear to be segmented at the vertical of the MUF. This pattern is an argument against a model in which the Urals are built on a typical East European crust. Moreover, in Fig. 2b, a lower crustal flake is observed by Thouvenot et al. (1995) from the fan reflections: this flake is located in the Uralian crustal root. Vertical reflections also mark this spot in Juhlin et al. (1995). From GEON's DSS results, the P-wave velocity inside this lower crustal flake is very low compared to the velocity at the same depth in the lower crust of the East European plate and of the Siberian plate: 6.55 km/s compared to 6.85 km/s. Such a low velocity — here at a depth of 35–40 km — is usually found at a depth of 20–30 km (Rudnick and Fountain, 1995). Moreover, GEON reports a V_P/V_S ratio of 1.68 compared to 1.75 at the same depth in the East European craton. So we should expect a less mafic and more felsic composition of this lower crustal flake. This could be a supplementary argument to consider that the Urals are formed on a plate of a different nature than the East European plate. A felsic composition of the lower crust beneath the Urals does not fit the hypothesis of Juhlin et al. (1995) according to which the crustal root of the Urals is a modified upper-mantle material. If we assume a middle-crust origin for this crustal flake, a piece of crust disappeared during the compressional episode that formed the Urals.

We can also compare our results with the URSEIS profile which was investigated by seismic reflection and refraction in the southern Urals (Knapp et al., 1996; Carbonell et al., 1996) about 500 km south of our profile but on a similar geological cross-section. From the explosion reflection profile, Knapp et al. (1996) find a Moho offset of about 4 km on the UFTZ, between the East European platform and the West Uralian zone: this result agrees with our teleseismic results which indicates that the structure of the crust and lithosphere is changing on the UFTZ. Further east, in the central Urals, Carbonell et al. (1996) find a high V_P/V_S ratio (1.9–2.0) in the upper crust which correlates with the Kraka lherzolitic klippe and with the Magnitogorsk volcanic arc and a low V_P/V_S ratio (1.6–1.7) in the middle and lower crust beneath the East Uralian zone. This result implies that the mafic bodies correlated to the volcanic arcs are not deeply rooted. The low V_P/V_S body is slightly shifted to the east as compared to GEON's results but it also implies a mineralogical composition difference (more silicic) of the lower crust in a piece of the Central Uralian crust.

The Uralian plate was shortened and deformed in between the East European plate to the west and the Siberian plate to the east. Our profile does not extend far enough to the east to delineate properly the Siberian plate but there is a suggestion of a change in crustal velocity when entering the eastern Uralian zone both on the inversion and in GEON's DSS profile.

The two high-velocity bodies shown by the teleseismic inversion near km 400 and km 500 appear to be rootless. The western block corresponds to the Tagil volcanic arc pinched between two conti-

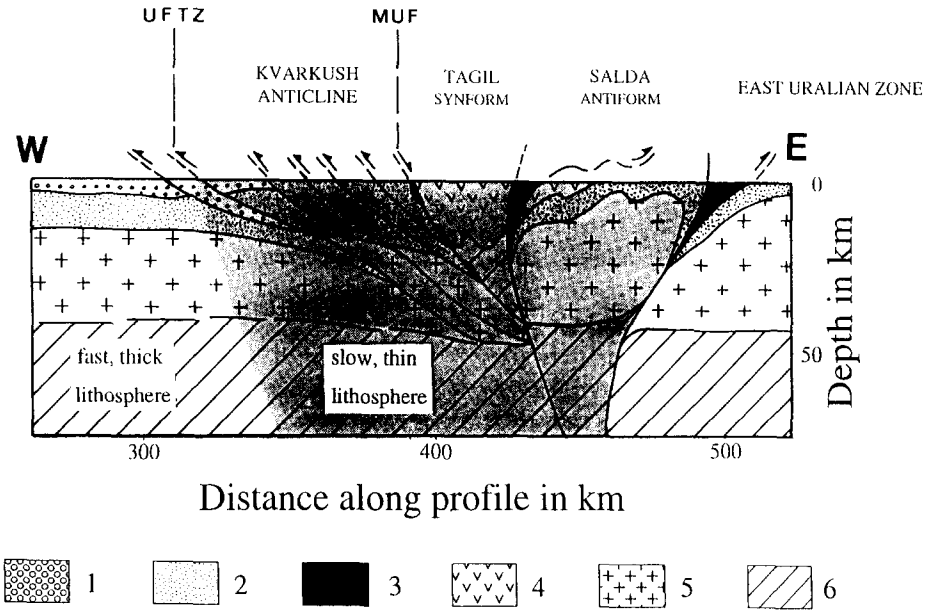

Fig. 8. Schematic crustal section from surface geology, CDP and wide-angle seismics with juxtaposition of the main lithospheric units deduced from teleseismics. The lower-velocity Uralian plate is shaded. *1* = Permian foredeep; *2* = Riphean to Palaeozoic sediments; *3* = peridotites and serpentinites (suture zones); *4* = volcanic island arcs; *5* = Precambrian basement; *6* = lithospheric mantle. The Uralian frontal thrust zone is labelled *UFTZ* and the Main Uralian fault is labelled *MUF*.

nental blocks. The easternmost high-velocity block could correspond to another suture resulting from a westward dipping subduction (Matte, 1995). This hypothesis seems to be confirmed by the URSEIS deep seismic vertical profile where the Magnitogorsk volcanic arc is underlain by continental crust (Carbonell et al., 1996). From these observations, we propose a schematic cross-section of the middle Urals as shown by Fig. 8.

Geological cross-sections usually imply a western boundary thrust of the Urals which is less steep than the lithospheric plate boundary deduced from teleseismics. It appears clearly that the Uralian orogenic lithosphere has an average velocity lower than the stable East European craton. This is probably due in part to the crystalline/sedimentary imbrication and to a modification of the deep lithosphere by the continental subduction process and by orogeny.

Despite the general agreement that the Urals result from the collision between two continents separated by island arcs, the precise positions of the sutures at depth and the identification of distinct crustal and lithospheric units are important to decipher the mechanism that led to the formation of this linear mountain belt. The seismic studies presented here and those from the southern Urals (project URSEIS) contribute to a better understanding of the deep structures that remain long after the collision between two continents.

Acknowledgements

Funded by Lithoscope, a project from the French Institut National des Sciences de l'Univers and by GEON, Moscow, Russia, this work has only been possible thanks to the Europrobe initiative. We thank Prof. David Gee and Prof. Karl Fuchs for their enthusiasm over bringing together eastern and western European teams. We thank Dr. Uli Achauer for his tests of the stability of the inversion with his new programs and L. Jenatton for her help. Leo Vinnik was kind enough to check this tomographic inversion and published it in Dokl. Akad. Nauk, 1996, p. 668. Europrobe contribution 101. INTAS grant #94-1857.

References

Aki, K., Christoffersson, A., Husebye, E.S., 1977. Determination of the three-dimensional seismic structure of the lithosphere. J. Geophys. Res. 82, 277–296.

Carbonell, R., Pérez-Estaún, A., Gallart, J., Diaz, J., Kashubin, S., Mechie, J., Stadtlander, R., Schulze, A., Knapp, J.H., Morozov, A., 1996. A crustal root beneath the Urals: wide-angle seismic evidence. Science 274, 222–224.

Egorkin, A., 1995. DSS cross-section of the Urals teleseismic profile. GEON, Moscow.

Ellsworth, W.L., 1977. Three-dimensional Structure of the Crust and Mantle Beneath the Island of Hawaii. Ph.D. thesis, Massachusetts Institute of Technology, Cambridge, 237 pp.

Evans, J.R., Achauer, U., 1992. Teleseismic velocity tomography using the ACH method: theory and application to continental scale studies. In: Iyer, H.M., Hirahara, K. (Eds.), Seismic Tomography: Theory and Practice. Chapman and Hall, London, pp. 319–360.

Hamilton, W., 1970. The Uralides and the motion of Russian and Siberian platforms. Geol. Soc. Am. Bull. 81, 2553–2576.

Herrin, E., 1968. Seismological tables for P phases. Bull. Seismol. Soc. Am. 58, 1193–1242.

Hurtig, E., Cermak, V., Haenel, R., Zui, V.I. (Eds.), 1992. Geothermal Atlas of Europe. Hermann Haack, Gotha, 156 pp.

Ivanov, S.N., Perfiliev, A.S., Efimov, A.A., Smirnov, G.A., Necheukhin, V.M., Fershtater, G.B., 1975. Fundamental features in the structure and evolution of the Urals. Am. J. Sci. 275, 107–130.

Juhlin, C., Kashubin, S., Knapp, J.H., Makovsky, V., Ryberg, T., 1995. Project conducts seismic reflection profiling in the Ural mountains. EOS 76, 193–197.

Kashubin, S.N., Rybalka, V.M., Sokolov, V.B., 1995. Location map and table of acquisition parameters of existing seismic lines. In: EUROPROBE — Urals Seismics proposal by Europrobe-Urals Research Group Univ. Uppsala.

Kissling, E., 1988. Geotomography with local earthquakes. Rev. Geophys. 26, 659–698.

Knapp, J.H., Steer, D.N., Brown, L.D., Berzin, R., Suleimanov, A., Stiller, M., Lüschen, E., Brown, D.L., Bulgakov, R., Kashubin, S.N., Rybalka, A.V., 1996. A lithosphere-scale seismic image of the Southern Urals from explosion source reflection profiling. Science 274, 226–228.

Kruse, S., McNutt, M., 1988. Compensation of Paleozoic orogens: a comparison of the Urals to the Appalachians. Tectonophysics 154, 1–17.

Lennykh, V.I., 1980. Metamorphic complexes of the Urals western slope. In: Ivanov, S.N. (Ed.), Pre-Ordovician History of the Urals (in Russian). Ural Sci. Centre, Sverdlovsk 6, 340.

Matte, P., 1995. Southern Uralides and Variscides: comparison of their anatomy and evolution. Geol. Mijnbouw 74, 151–166.

Ministry of Geology SSSR, 1966. Geological map of Urals: Nizhniy Tagil, scale 1/100,000, Moscow.

Rudnick, R.L., Fountain, D.M., 1995. Nature and composition of the continental crust: a lower crustal perspective. Rev. Geophys. 33, 267–310.

Ryzhiy, B.P., Druzhinin, V.S., Yunusov, F.F., Anayin, I.V., 1992. Deep structure of the Urals region and its seismicity. Phys. Earth Planet. Inter. 75, 185–191.

Thouvenot, F., Kashubin, S.N., Poupinet, G., Makovskiy, V.V., Kashubina, T.V., Matte, Ph., Jenatton, L., 1995. The root of the Urals from wide-angle reflection seismics. Tectonophysics 250, 1–13.

Zonenshain, L.P., Korinevsky, V.G., Kazmin, V.G., Pechersky, D.M., Khain, V.V., Matveenkov, V.V., 1984. Plate tectonic model of the South Urals development. Tectonophysics 109, 95–135.